PROCEEDINGS OF SCIENCE

The Cosmic-ray Anisotropy Observed by YBJ-HA Experiment

Yingying Guo*[ab], Shiping Zhao[a], Yi Zhang[ab], Youliang Feng[a], Yuhua Yao[ac], Jiancheng He[ab], Yiqing Guo[a], Cheng Liu[a] and Hongbo Hu[a]

[a] *Institute of High Energy Physics, Chinese Academy of Sciences*
No.19B Yuquan Road, Shijingshan District, Beijing, 100049, P.R. China
[b] *University of Chinese Academy of Sciences*
No.19A Yuquan Road, Shijingshan District, Beijing, 100049, P.R. China
[c] *College of Physical Science and Technology, Sichuan University*
N.29 Wangjiang Road, Jiuyanqiao, Wuhou District, Chengdu City, Sichuan Province, 610064, P.R. China

E-mail: yyguo@ihep.ac.cn

The Yangbajing Hybrid Array(YBJ-HA) has accumulated over 0.8 billion cosmic-ray events from December 2016 to June 2018, which is a test array for Large High Altitude Air Shower Observatory Square Kilometer Array(LHAASO-KM2A). The large-scale anisotropy is observed by using this data. The global sidereal anisotropy exhibits an excess and a deficit with an amplitude of $\sim 10^{-3}$ at the median energy of 15TeV, and there is no time dependence of the structure discovered during the operation. Besides, the observed variations in the anti-sidereal and extended-sidereal time frames are at the level of $\sim 10^{-5}$, which ensure the precise measurement of the sidereal anisotropy.

36th International Cosmic Ray Conference -ICRC2019-
July 24th - August 1st, 2019
Madison, WI, U.S.A.

*Speaker.

PoS(ICRC2019)493

1. Introduction

The studies of Galactic cosmic rays (GCRs) have identified that the arrival directions of the GCRs are highly isotropic; weak but significant anisotropies are persistently observed at various angular scales, with the relative amplitude varying from $\sim 10^{-4}$ to 10^{-3}. In the past decades, observations by the ground-based experiments have made great progress. Numerous measurements of the two-dimensional high-precision CR anisotropy have been published [1, 2, 3, 4, 5, 6, 7, 8, 9, 10, 11, 12, 13, 14, 15], ranging from hundreds of GeV up to several PeV. The all-sky picture and energy evolution of the GCR anisotropy are revealed by combining with the data of both northern and southern hemispheres.

In the anisotropy map, we observed a large-scale dipole-like feature and studied its energy dependence. At energy below tens of TeV, two broad structures are visible: one excess close to the direction of the helio-tail with right ascension (R.A.) = 110° (namely known as “tail-in" region) and a deficit pointing towards the Galactic North pole with R.A.= 220° (also referred to “loss-cone" region). Apart from the above two components, a new excess in the direction of the cygnus region is reported by the Tibet air shower array [1]. But at higher energies, the CR arrival distributions are total altered: the deficit structure appears at R.A. $\sim 80°$, while the corresponding excess feature pointing to the Galactic center shifts to R.A. $\sim 260°$.

The GCR anisotropy is conventionally measured in one dimension, i.e. the projection of the two-dimensional map onto the R.A. axis. The one-dimension anisotropy can be fitted by the first-order harmonic function, and then be quantitatively described by the amplitude and phase. Meanwhile, the amplitude and phase are energy dependent. The amplitude is found to grow with energy from ∼0.1 to ∼10 TeV. But above that energy range, the amplitude slowly drops until ∼100 TeV. Further, the morphology of anisotropy changes around hundreds of TeV, and the predicted amplitude gradually increase with energy from hundreds of TeV to PeV[16].

Various theoretical models have been proposed to explain the observed large-scale anisotropy. One of well-known origin is the so-called Compton-Getting effect[17]. It is induced by the relative motion of the observer to the CR rest frame. Because this effect is of kinematic origin, the amplitude of anisotropy does not vary with CR energy.

In addition, the diffusion process itself also predicts a dipole anisotropy. It has long been recognized that the CRs propagate in the Galaxy by frequently scattering with the random magnetic turbulence, which could be described by diffusion equation. The conventional steady-state CR diffusion model predicts a large-scale dipole anisotropy, which results from the non-uniform distribution of CR sources. However, the predicted amplitude is proportional to the diffusion coefficient, which is well beyond the actual measurements[18]. And the direction of the predicted dipole always points to the direction of the Galactic center. Therefore the conventional model can neither reproduce the evolution of amplitude nor phase.

To ease up above inconsistencies, modifications based on the conventional diffusion model have been suggested and most of which attribute to the ensemble fluctuations of CR sources or nearby sources [19, 20, 21, 22], spatial-dependent propagation [18, 23, 24], etc. A recent work [16] describes CR energy spectra and anisotropy simultaneously, by combining spatial-dependent propagation with local source models. This study provides a probe to identify source(s) of GCRs by measurement of spectrum and anisotropy.

A precise observation of anisotropy from LHAASO-KM2A is potential to shed light on these puzzles. As a testing array of KM2A, YBJ-HA has been in stable operation for about two years. we present the CR large-scale anisotropy as well as the investigations on long-term stability and systematic errors.

2. Experiment data and simulation

YBJ-HA is located at the YangBaJing international cosmic ray observatory, Tibet, China. It consists of 115 scintillation detectors(SDs) and 16 underground water Cherenkov muon detectors(MDs). The layout is presented in Figure 1(a). More details have been reported in [25, 26]. Moreover, all detectors adopted both the electronics and white rabbit clock synchronization system designed for LHAASO-KM2A. YBJ-HA has been running since December 2016. The long time span of operation provides KM2A an effective monitoring and debugging platform. The direction of event is reconstructed by fitting a plane to the front of the air shower, according to the arrival time and quantity of charge of secondary particles recorded in different SDs.

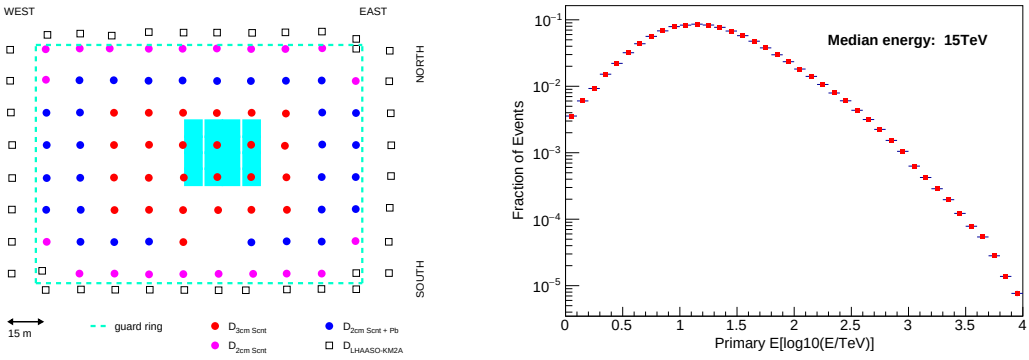

(a) (b)

Figure 1: Left:The layout of YBJ-HA. Scintillation detectors(SDs) is denoted as circles. Different colors repersent the different depths of scintillators. Red circles are detectors with 3 cm thick scintillators while pink circles are detectors with 2 cm thick scintillators, and blue circles are detectors with 2 cm thick scintillators and lead plates. The squares are the prototype detectors of the LHAASO-KM2A. Cyan shaded area is the water Cherenkov muon detector array buried 2.5 m underground. SDs inside the guarding ring is denoted as inner SDs. Right: The fraction of events as a function of the simulated primary energy for the data set used in this analysis.

The full simulation is completed based on CORSIKA-74005 and GEANT4 package for CRs with energy ranging from 1 TeV to 10 PeV. QGSJET2 and GHEISHA interaction models are used at high and low energy range separately to simulate the development of extensive air shower(EAS). GEANT4 simulates the detector response. The cosmic-ray spectrum adopts Gaisser-Hillas Model [27]. The observed muon lateral distribution [26] has verified the reliability of the simulation.

The data set used in this analysis is the events satisfying the following criteria:

1) The average time residuals in the direction reconstruction must be smaller than 3ns.

2) The top four scintillation detectors with the largest charge must be inside the guarding ring.

3) The zenith angle is less than 60°.

These events are divided into four phases shown in Table 1, according to the running status. The fraction of events as a function of the simulated primary energy for the selected data set is shown in Figure 1(b), and the median energy is 15TeV.

Table 1: Data phase and the their respective number of events for analysis

Phase	Date	Number of Events
1	2016032-2017052	1.081×10^8
2	2017052-2017129	1.361×10^8
3	2017160-2017305	2.701×10^8
4	2018006-2018186	2.886×10^8

To analyze the data, the all-distance equi-zenith angle method [28] is adopted, which has been proved to be sensitive to probe large-scale anisotropy. The field of view is divided into small grid of $1^\circ \times 2^\circ$ in zenith and azimuth angle separately. As for the equatorial coordinate, it is divided into grid of $2^\circ \times 2^\circ$. In order to study the large scale structure of anisotropy, the two-dimensional (2D) map in the equatorial coordinate is smooth by 30° top-hat function. In order to quantify the amplitude of the anisotropy, an one-dimensional(1D) profile is obtained along R.A. axis, by averaging the relative intensities in all declination before smoothing. The R.A. is binned by 15° for 1D analysis. The first-order harmonic function in the form of

$$R(\alpha) = 1 + Acos(\alpha - \phi)$$

is applied to fit the 1D profile and estimate the amplitude.

3. Results

Figure 2 shows the significance map and relative intensity map of the sidereal anisotropy. The intensity map, shown in the middle panel in Figure 2 is characterized by a large excess from 30° to 90° and a deficit from 150° to 230°. From the significance map in the top panel of Figure 2, both regions can be observed with a significance more than 5σ. The projection of the relative intensity in right ascension is shown in the bottom panel, the amplitude is at the level of $\sim 0.1\%$. The observed large-scale anisotropy is stable over the data taking period as shown in Figure 3, other experiments such as [6, 14] also find no evidence for a time dependence of the structure.

4. Systematic checks

A dipole solar anisotropy is observed due to the Earth orbits around the Sun. The strongest excess is in the direction of the Earth motion and a corresponding deficit in the opposite direction. This motion in principle does not affect the anisotroy in sidereal time. However, the seasonal variation in solar time can manifest itself as an anisotropy in sidereal time and vice versa. Therefore, the anisotropy in anti-sidereal time and extended-sidereal time is employed to estimate the mutual effect between solar and sidereal anisotropy. Because there is no expected anisotropy in both anti-sidereal time and extended-sidereal time, the observed variations in these time frames can estimate the systematic error.

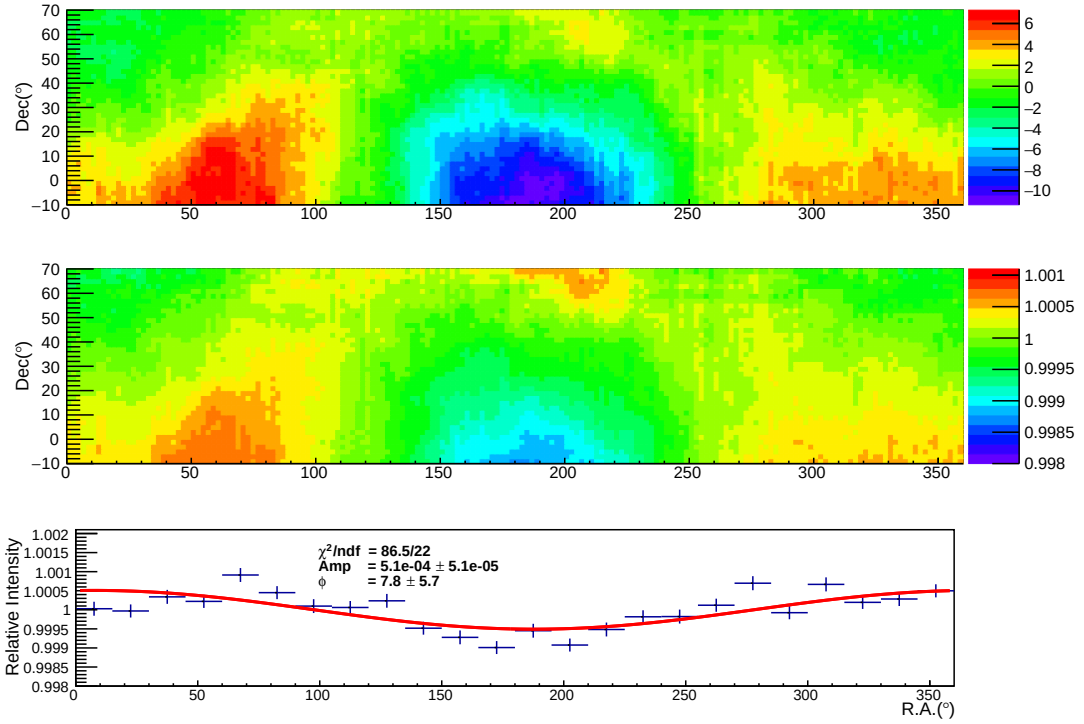

Figure 2: The large-scale anisotropy at 15TeV by the YBJ-HA. The 2D maps are smoothed with a 30° top-hat function. The top panel is the significance map, the middle panel displays the relative intensity map, while the bottom one shows the 1D projection the relative map onto the R.A. axis. The red curve shows the first-order harmonic fitting to the data.

Figure 4 is the projection of the relative intensity in R.A. for the different time frames. The amplitude of the anisotropy in the solar time is at the $\sim 10^{-4}$ level as shown in the top panel. The anisotropy in the anti-sidereal time is in the middle panel and the bottom panel shows anisotropy in the extended-sidereal time. The amplitudes in the both anti-sidereal and extended-sidereal time frames are at the $\sim 10^{-5}$, which indicates the solar anisotropy influence on the sidereal anisotropy is small, and vice versa. Our anisotropy measurement stands still while considering the small systematic error.

5. Discussion

Using two-year collections of events from YBJ-HA at a median energy of 15TeV, we presented the anisotropy results in the northern sky. The amplitude of sidereal anisotropy is measured at a level of $\sim 0.1\%$, this result appears to be consistent with previously measured cosmic-ray anisotropy. Moreover, no time dependence of the morphology of sidereal anisotropy is measured during the operation time at tens of TeV.

Although the anisotropy of cosmic rays has been reported in several experiments, the interpretation of the origin is not confirmed. The excess may originates from the artifact of the heliospheric magnetic field. However, the scale of heliospheric magnetic field is much smaller than the gyrora-

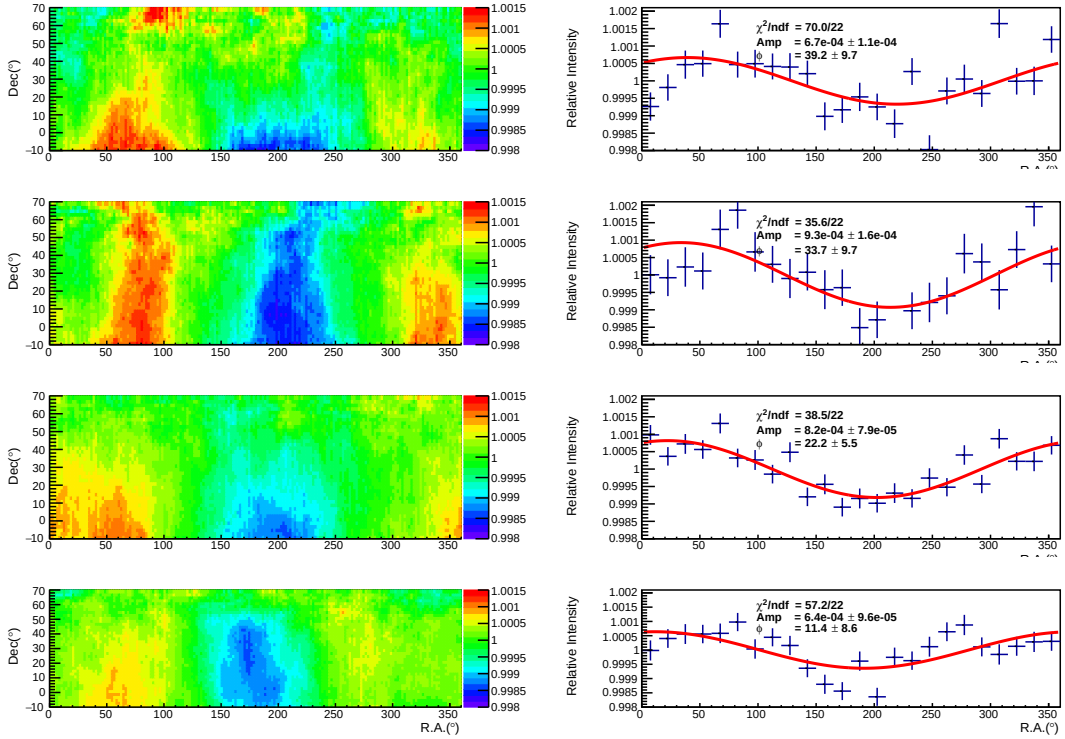

Figure 3: The sidereal anisotropy in different phases: the phase number increase from 1 to 4 as the panel from top to bottom. The left panels are the relative intensity sky maps, the one-dimensional projections to R.A. are in the right panels, and the data are shown with statistic uncertainties.

dius of tens of TeV cosmic rays in a 0.1μG. Other work[16] investigates on the probability of the contribution from nearby sources, such as geminga, which may connect the cosmic-ray spectrum characters with the anisotropy.

As the pre-testing array of LHAASO-KM2A, the successful observation of CR anisotropy confirmed the stability of the detectors. The future completed KM2A, covering an area of 1 km^2, will allow us to determine the variation of cosmic-ray anisotropy from tens of TeV to tens of PeV. The energy dependence of anisotropy will provide evidence of the source and constrain the propagation process.

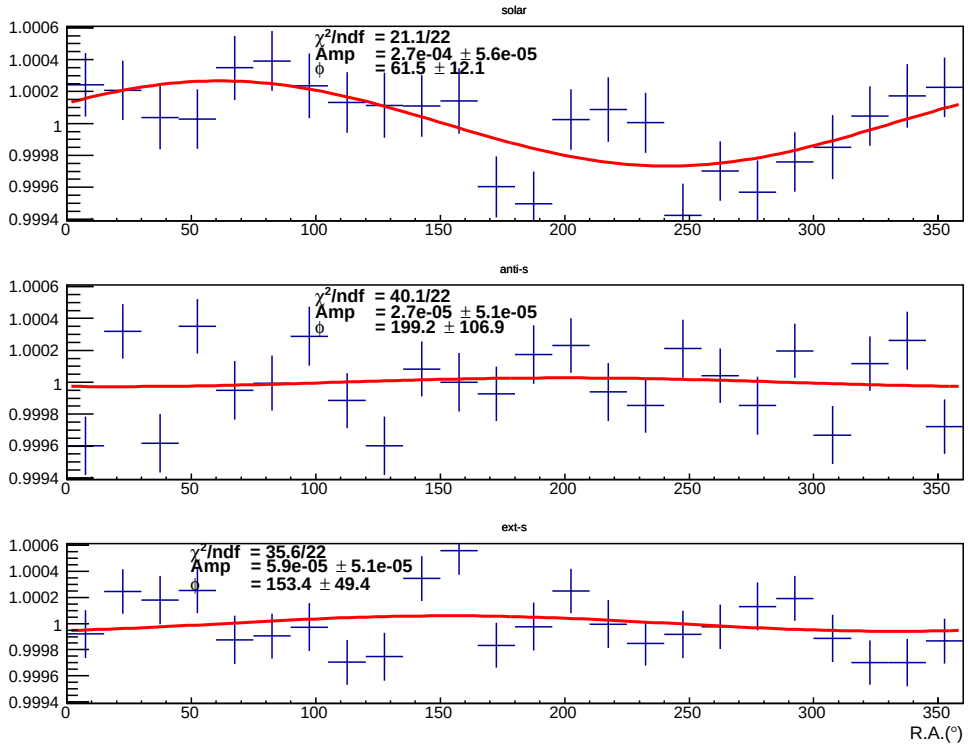

Figure 4: The projection of the relative intensity onto the R.A. axis in the solar(top), anti-sideral(middle) and extended-sideral(bottom) time frames.

References

[1] M. Amenomori, S. Ayabe, X. J. Bi, et al. Anisotropy and Corotation of Galactic Cosmic Rays. *Science*, 314:439–443, October 2006.

[2] M. Amenomori, S. Ayabe, S. W. Cui, et al. Large-Scale Sidereal Anisotropy of Galactic Cosmic-Ray Intensity Observed by the Tibet Air Shower Array. ApJ, 626:L29–L32, June 2005.

[3] G. Guillian, J. Hosaka, K. Ishihara, et al. Observation of the anisotropy of 10TeV primary cosmic ray nuclei flux with the Super-Kamiokande-I detector. Phys. Rev. D, 75(6):062003, March 2007.

[4] A. A. Abdo, B. Allen, T. Aune, et al. Discovery of Localized Regions of Excess 10-TeV Cosmic Rays. *Physical Review Letters*, 101(22):221101, November 2008.

[5] A. A. Abdo, B. T. Allen, T. Aune, et al. The Large-Scale Cosmic-Ray Anisotropy as Observed with Milagro. ApJ, 698:2121–2130, June 2009.

[6] M. Amenomori, X. J. Bi, D. Chen, et al. On Temporal Variations of the Multi-TeV Cosmic Ray Anisotropy Using the Tibet III Air Shower Array. ApJ, 711:119–124, March 2010.

[7] R. Abbasi, Y. Abdou, T. Abu-Zayyad, et al. Measurement of the Anisotropy of Cosmic-ray Arrival Directions with IceCube. ApJ, 718:L194–L198, August 2010.

[8] R. Abbasi, Y. Abdou, T. Abu-Zayyad, et al. Observation of Anisotropy in the Arrival Directions of Galactic Cosmic Rays at Multiple Angular Scales with IceCube. ApJ, 740:16, October 2011.

[9] R. Abbasi, Y. Abdou, T. Abu-Zayyad, et al. Observation of Anisotropy in the Galactic Cosmic-Ray Arrival Directions at 400 TeV with IceCube. ApJ, 746:33, February 2012.

[10] M. G. Aartsen, R. Abbasi, Y. Abdou, et al. Observation of Cosmic-Ray Anisotropy with the IceTop Air Shower Array. ApJ, 765:55, March 2013.

[11] B. Bartoli, P. Bernardini, X. J. Bi, et al. Medium scale anisotropy in the TeV cosmic ray flux observed by ARGO-YBJ. Phys. Rev. D, 88(8):082001, October 2013.

[12] A. U. Abeysekara, R. Alfaro, C. Alvarez, et al. Observation of Small-scale Anisotropy in the Arrival Direction Distribution of TeV Cosmic Rays with HAWC. ApJ, 796:108, December 2014.

[13] B. Bartoli, P. Bernardini, X. J. Bi, et al. ARGO-YBJ Observation of the Large-scale Cosmic Ray Anisotropy During the Solar Minimum between Cycles 23 and 24. ApJ, 809:90, August 2015.

[14] M. G. Aartsen, K. Abraham, M. Ackermann, et al. Anisotropy in Cosmic-Ray Arrival Directions in the Southern Hemisphere Based on Six Years of Data from the IceCube Detector. ApJ, 826:220, August 2016.

[15] M. Amenomori, X. J. Bi, D. Chen, et al. Northern Sky Galactic Cosmic Ray Anisotropy between 10 and 1000 TeV with the Tibet Air Shower Array. ApJ, 836:153, February 2017.

[16] Wei Liu, Yi-Qing Guo, and Qiang Yuan. Indication of nearby source signatures of cosmic rays from energy spectra and anisotropies. *arXiv e-prints*, page arXiv:1812.09673, Dec 2018.

[17] Arthur H Compton and Ivan A Getting. Theoretical Physics. 47(11):817–821, 1935.

[18] C. Evoli, D. Gaggero, D. Grasso, and L. Maccione. Common Solution to the Cosmic Ray Anisotropy and Gradient Problems. *Physical Review Letters*, 108(21):211102, May 2012.

[19] A. D. Erlykin and A. W. Wolfendale. The anisotropy of galactic cosmic rays as a product of stochastic supernova explosions. *Astroparticle Physics*, 25:183–194, April 2006.

[20] P. Blasi and E. Amato. Diffusive propagation of cosmic rays from supernova remnants in the Galaxy. II: anisotropy. J. Cosmology Astropart. Phys., 1:11, January 2012.

[21] L. G. Sveshnikova, O. N. Strelnikova, and V. S. Ptuskin. Spectrum and anisotropy of cosmic rays at TeV-PeV-energies and contribution of nearby sources. *Astroparticle Physics*, 50:33–46, December 2013.

[22] W. Liu, X.-J. Bi, S.-J. Lin, B.-B. Wang, and P.-F. Yin. Excesses of cosmic ray spectra from a single nearby source. Phys. Rev. D, 96(2):023006, July 2017.

[23] N. Tomassetti. Origin of the Cosmic-Ray Spectral Hardening. ApJ, 752:L13, June 2012.

[24] Y.-Q. Guo, Z. Tian, and C. Jin. Spatial-dependent Propagation of Cosmic Rays Results in the Spectrum of Proton, Ratios of P/P, and B/C, and Anisotropy of Nuclei. ApJ, 819:54, March 2016.

[25] Zhen Wang, Yiqing Guo, Hui Cai, et al. Performance of a scintillation detector array operated with LHAASO-KM2A electronics. *Exp Astron*, (45):363–377, 2018.

[26] You-liang Feng, Yi Zhang, Hong-bo Hu, and Cheng Liu. Lateral distribution of EAS muons measured at the primary cosmic ray energy around 100TeV *. *Chinese Physics C*, 37(1):1–6, 2019.

[27] T. K. Gaisser, T. Stanev, and S. Tilav. Cosmic ray energy spectrum from measurements of air showers. *Front. Phys.*, 8(6):748–758, 2013.

[28] M. Amenomori, S. Ayabe, D. Chen, et al. A Northern Sky Survey for Steady Tera–Electron Volt Gamma-Ray Point Sources Using the Tibet Air Shower Array. *The Astrophysical Journal*, 633:1005–1012, 2005.